Theoretical Insight into the Photodegradation of a Disulfide Bridged Cyclic Tetrapeptide in Solution and Subsequent Fast Unfolding−Refolding Events

Xuebo Chen,*,† Lianghui Gao,† Weihai Fang,*,† and David Lee Phillips*,‡

Department of Chemistry, Beijing Normal University, Xin-wai-da-jie #19, Beijing 100875, P. R. China, and Department of Chemistry, The University of Hong Kong, Pokfulam Road, Hong Kong S.A.R., P. R. China

Received: January 13, 2010; Revised Manuscript Received: March 11, 2010

We report the photoinduced peptide bond (C−N) of an amide unit and S−S bond fission mechanisms of the cyclic tetrapeptide [cyclo(Boc-Cys-Pro-Aib-Cys-OMe)] in methanol solvent by using high-level CASSCF/CASPT2/Amber quantum mechanical/molecular mechanical (QM/MM) calculations. The subsequent energy transport and unfolding−refolding events are characterized by using a semiempirical QM/MM molecular dynamics (MD) simulation methodology that is developed in the present work. In the case of high-energy excitation with <193 nm light, the tetrapeptide molecule in the $^1n\pi^*$ surface overcomes two barriers with ∼10.0 kcal/mol, respectively, and uses energy consumption for breaking the hydrogen bond as well as the N−C bond in the amide unit, ultimately leading to the ground state via a conical intersection of CI (S_{NP}/S_0) by structural changes of an increased N−C distance and a O−C−C angle in the amide unit (a two-dimensional model of the reaction coordinates). Following this point, relaxation to a hot molecule with its original structure in the ground state is the predominant decay channel. A large amount of heat (∼110.0 kcal/mol) is initially accumulated in the region of the targeted point of the photoexcitation, and more than 60% of the heat is rapidly dissipated into the solvent on the femtosecond time scale. The relatively slower propagation of heat along the peptide backbone reaches a phase of equilibration within 3 ps. A 300 nm photon of light initiates the relaxation along the repulsive $S_{\sigma\sigma}(^1\sigma\sigma^*)$ state and this decays to the CI ($S_{\sigma\sigma}/S_0$) in concomitance with the separation of the disulfide bond. Once cysteinyl radicals are generated, the polar solvent of methanol molecules rapidly diffuses around the radicals, forming a solvent cage and reducing the possibility of close contact in a physical sense. The fast unfolding−refolding event is triggered by S−S bond fission and powered by dramatic thermal motion of the methanol solvent that benefits from heat dissipation. The β-turn opening (unfolding) can be achieved in about 120 ps without the inclusion of the time associated with the photochemical steps and eventually relaxes to a 3_{10}-helix structural architecture (refolding) within 200 ps.

Introduction

Many processes by which proteins are degraded are not well understood. Ciechanover, Hershko, and Rose discovered one of the cell's most important cyclical processes, regulated protein degradation, and found that the cell functions as a highly efficient checking station where proteins are built up and broken down at fast rates.[1−4] A better understanding of how proteins interact with ultraviolet light has important implications in many fields such as laser surgery and the photodegradation of polymers.[5] While the nature of the ground-state structures of a number of proteins have become well-characterized, less is known about their excited states and their subsequent processes. As a model for the fundamental repeating unit in the backbone of proteins, the photolysis of amides in the gas phase and in solution environments have been extensively studied by different spectroscopy techniques and theoretical calculations.[6−15] Our previous investigations showed that simple aliphatic and aromatic amides were initially excited by ∼193 nm UV light irradiation to the $^1n\pi^*$ surface, resulting in promoting a nonbonding electron of oxygen in O═C−NH−R(H) to an antibonding π orbital, and this excitation eventually leads to radical fragments or a hot molecule in the ground state.[6,7] Although the fission of the C−N bond was proposed to be the primary photochemical step,[6−15] only small quantum yields of the CHO and NH_2 radical pairs were observed by recent real-time femtosecond experiments.[16] This finding reveals that 50% of the radical pairs undergo recombination, leading to a hot molecule in the ground state, and ∼80% of the amide molecules finally convert the electronic excitation energy to vibrational excitation that is effectively dissipated to the solvent through vibrational relaxation in just a few picoseconds.[16]

In the Protein Data Bank (PDB), more than 80% of the proteins contain a disulfide bond, which is an important inert building block.[17] The redox state of protein disulfide bonds is regulated by the cell redox status and can have consequences that govern the stability and functions of proteins (i.e., folding and transport).[18−20] The oxidative disulfide bond (−S−S−) in peptides/proteins has a low dissociation energy and is easily cleaved when excited by ultraviolet light, and the cleavage can be followed by further conformational dynamics.[21−25] The folding or unfolding events initiated by a photocleavable disulfide bridge can be monitored by different experimental approaches including temperature jump,[26−28] resonance Raman,[29,30] and fluorescence techniques.[31,32] However, the most commonly used spectroscopic methods, time-resolved electronic absorption and fluorescence, are very insensitive probes of molecular structure. Hamm and co-workers applied the methods of

* To whom correspondence should be addressed. E-mail: xuebochen@bnu.edu.cn (X.C.); fangwh@bnu.edu.cn (W.F.); phillips@hkucc.hku.hk (D.L.P.).
† Beijing Normal University.
‡ The University of Hong Kong.

10.1021/jp1003616
Published on Web 03/29/2010

transient IR spectroscopy and transient two-dimensional (2D)-IR spectroscopy to investigate peptides with built-in photoswitches, such as azobenzene,[33,34] a thio-peptide unit,[35] and a photocleavable disulfide bridge.[24,25] These experimental studies were able to follow the structural changes of the peptides over a wide time-window from a few picoseconds to many hundreds of microseconds.[24,25,33−35] Although important dynamical processes concerning peptide folding (unfolding) have been characterized by powerful time-resolved laser techniques, detailed information regarding the mechanism(s) of the structural changes still needs further elucidation from the relaxation pathways of the photochemical steps and dynamic simulations.[36]

In this work, we investigate the mechanism of photodegradation of a disulfide bridged cyclic tetrapeptide [cyclo(Boc-Cys-Pro-Aib-Cys-OMe)] in a methanol matrix and its subsequent unfolding-refolding events triggered by S−S bond fission. There are two different decay channels to account for the photodegradation of the tetrapeptide: C−N and S−S bonds fission upon irradiation by shorter and longer wavelengths of ultraviolet light, respectively. The amide group (−CO−NH_2−) is ubiquitous and an important chromophore that is able to absorb shorter wavelength UV light. The S−S bond is cleaved once the tetrapeptide molecule is promoted to the repulsive $^1\sigma\sigma^*$ excited state surface upon irradiation of longer UV light. The relaxation paths for C−N and S−S bonds fission are mapped, respectively, by employing CASSCF/CASPT2/Amber calculations and subsequent energy transport, and conformational changes of unfolding-refolding are characterized by using the methodology of semiempirical quantum mechanical/molecular mechanical (QM/MM) molecular dynamics (MD) simulation that is developed in this work.

Computational Details

To mimic the solvent environment of peptide, we built a methanol solvent box positioned within 10 Å from any given atom of the tetrapeptide [cyclo(Boc-Cys-Pro-Aib-Cys-OMe)] using the xleap module of the Amber[37] software package. We noted that the corresponding experiments were done in solvent of acetonitrile.[24,25] However, the solvent in the present work is described by using classic point charge (MM subsystem) from theoretic viewpoints and functions as vibrational energy reservoir. The solvent of methanol is able to similarly simulate the electric field of a point charge that can be obtained from coulomb's law and energy reservoir. Therefore, the replacement of acetonitrile by methanol does not make a principle difference. The full system was treated within periodic boundary conditions in three dimensions. A cutoff radius of 12 Å was used for the real space part of the electrostatic interactions and the van der Waals term. The Amber force field parameters were used in the present work. Fifty thousand steps of energy minimization were performed with 10 000 step intervals. After 50 000 steps of energy minimization, the system was subjected to a 1 ns long equilibration in the NPT ensemble[38] at a normal ambient temperature (T = 298 K) and pressure (p = 1 atm). All MM MD simulations were performed with the free of charge program NAMD[39] and the molecular visualization program VMD.[40]

The above classical MD simulations generated configurations for use in subsequent QM/MM calculations. Scheme 1 shows our QM/MM computational strategy. In the present work, we use the CASPT2//CASSCF/Amber (QM/MM) protocol to compute the potential energy surface of the photochemical steps where CASSCF and CASPT2 calculations are performed by the Gaussian[41] and Molcas[42] programs and the Amber force field (MM subsystem) is treated by the Tinker[43] tool packages. The

SCHEME 1: Simple Diagram of the QM/MM Computational Strategy for Finding the Energy Profiles of the Disulfide-Bridged Tetrapeptide [Cyclo(Boc-Cys-Pro-Aib-Cys-OMe)][a]

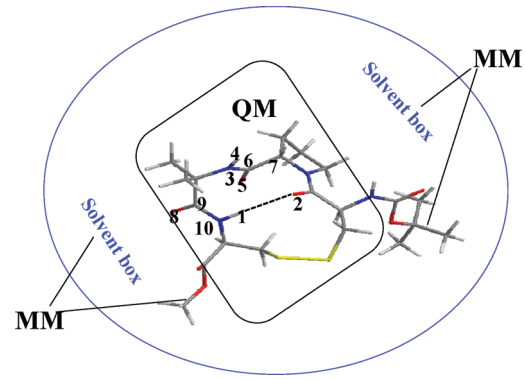

[a] QM subsystems include all of the atoms in the rectangle; Boc-NH− and −CO-OMe groups as well as all of the molecules of methanol in the solvent box are treated by MM.

interface between the QM and MM subsystems was coded by Ferré and his co-workers[44] and commercialized together with the MOLCAS[42] program. The present QM/MM calculations for the photochemical steps are based on a hydrogen link atom scheme where the frontier is placed between the QM and the MM subsystem ((Boc-H)N−C(Cys) and (Cys)C−C(O-OMe) bonds are cut, respectively (see Scheme 1 and the Supporting Information). The ab initio QM portion of the calculation was done at the CASSCF level with a 10e/9o active space. The orbitals and electrons in the active space originate from the C═O π, π^*, C−N σ, σ^* and n lone pair in the peptide plane of C6O5−N3H4 (see Scheme 1 for numbering scheme) as well as the C═O π, π^* in the peptide plane of C9O8−N10H1 and the S−S σ, σ^*. The MM part of the calculation was treated by the Amber force field using the standard or reparameterized potentials. To account for the dynamical electron correlation effects, the refined single-point energy is recalculated at the multiconfiguration second-order perturbation theory level (CASPT2) using a two-root state-averaged CASSCF (10e/9o) zeroth-order wave function. All CASPT2 calculations are performed using the MOLCAS 7.0 suite of programs.[42]

An efficient semiempirical QM/MM MD simulation method is developed to describe energy transport and unfolding-refolding dynamics. This method overcomes the shortcomings of MM MD not being able to describe the formation and breaking of the chemical bond, and significantly decreases the computational cost in comparison with *ab initio* MD simulations. All of the 68 atoms of the peptide were treated as the quantum subsystem in semiempirical QM/MM MD simulations. The semiempirical Hamiltonian for interactions between the QM atoms is PM6.[45] In the case of semiempirical simulations at the PM6 level of theory, the configuration interaction (CI) resulting from the mixing of four microstates was used to describe the biradical character of the S−S bond in the peptide.[45] A biradical calculation done without CI would be meaningless. On the other hand, PM6 represents a large change from earlier NDDO methods, and thus improve the prediction of hydrogen bonds from simple bonding of the type to stronger bonds of the type found in the amino acids.[45] The MM subsystem is composed of all of the solvent methanol molecules. The Amber force field with supplementation of Gaff parameters was used to calculate the interactions between the MM atoms. The QM/MM interactions include van der Waals and electrostatic interactions. For

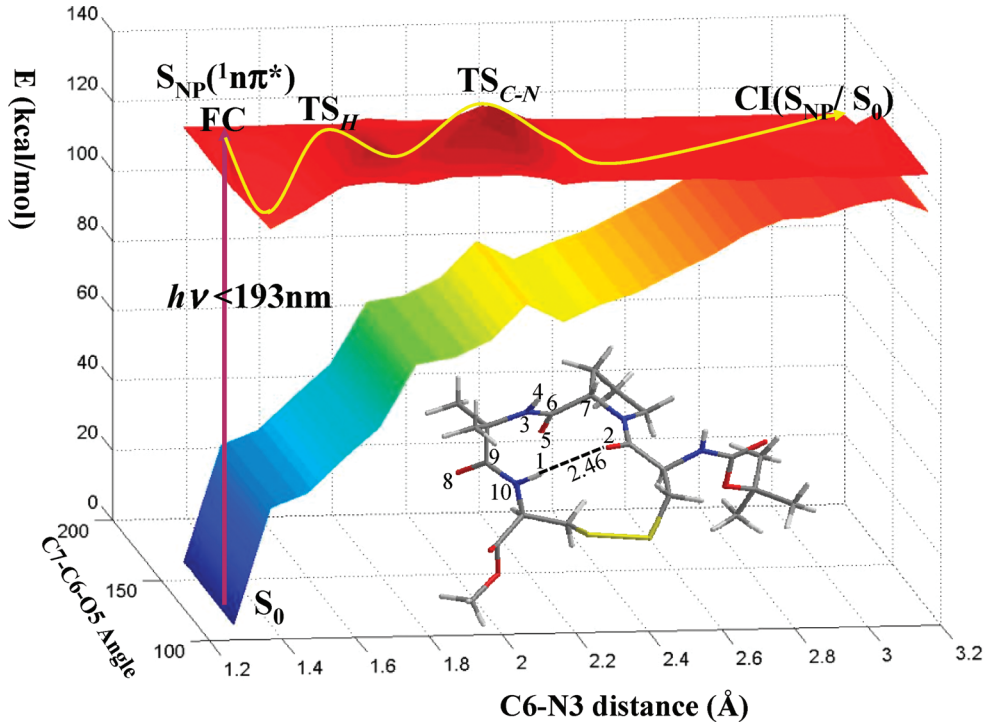

Figure 1. Schematic diagram of the energy profiles along the relaxation pathways for high energy excitation (<193 nm) that promotes the tetrapeptide to populate on the surface of the $^1n\pi^*$ transition and further drives the molecule to overcome two barriers (TS_H and TS_{C-N}) and then to relax to CI (S_{NP}/S_0).

electrostatic interactions, we first fit the electrostatic potential from the QM calculations and obtained the effective charge on each QM atom. Then we calculated the Coulomb interactions between the point charges of the QM atoms and the point charges of MM atoms, i.e.,

$$\langle\Psi| - \sum_{i}^{N} \sum_{\beta\in \mathrm{MM}} \frac{q_\beta}{r_{\beta i}} + \sum_{\alpha\in \mathrm{QM},\beta\in \mathrm{MM}} \frac{Z_\alpha q_\beta}{r_{\alpha\beta}} |\Psi\rangle = \sum_{\alpha\in \mathrm{QM},\beta\in \mathrm{MM}} \frac{Q_\alpha q_\beta}{r_{\alpha\beta}}$$

Here N is the total number of electrons of each QM atom, Z_α is the charge of the nuclei of the QM atoms, q_β is the point charge of the MM atom from the Amber force field, and Q_α is the electrostatic potential fitted point charge of the QM atom. The MD simulations are performed in a NVT ensemble using the Tinker tool packages.[43] One MD time step is set to be 0.2 fs, and the temperature is 298 K. See the Supporting Information for further computational details.

Results and Discussion

High-Energy Excitation (193 nm) Relaxation Pathway upon n→π* Transition of the Amide Chromophore. It is well established that $^1n\pi^*$ excited state is a precursor state for the C−N bond fission of amides.[6−15] To account for the photochemical behavior of the C−N bond cleavage induced by an n→π* transition of a tetrapeptide in a solution environment, we computed two different potential energy surfaces originating from excitation of the amide unit of C6O5−N3H4 and C9O8−N10H1 (see Figure 1 for numbering scheme), respectively. As expected, almost the same energy profiles were obtained by using CASSCF/Amber (QM/MM) optimizations. This implies that the peptides/proteins undergo the same relaxation mechanism no matter which amide unit is excited in the photoinitiation step upon irradiation of short wavelength UV light (i.e., less than 193 nm). Herein we only report the energy profile of an n→π* transition for the amide unit of C6O5N3H4 as an example to elucidate the decay mechanism of the tetrapeptide upon high energy excitation. The strong intramolecular hydrogen bond H1−O2 with 2.46 Å in the ground state of tetrapeptide forces the Boc-Cys-Pro and Aib-Cys-OMe residues to get closer and adopt a rigid architecture. This leads to the formation of a biofunctional β-turn supersecondary structure[46a] that has a strong intramolecular hydrogen bond between the i and $i + 3$ residues in its native state.[46b] Photoexcitation perturbation deviates the tetrapeptide from its native state by weakening the H1−O2 hydrogen bond from 2.46 Å in S_0 to 2.76 Å at the S_{NP} ($^1n\pi^*$) minimum. The evolution from the FC region causes the peptide plane (C7−C6−O5−N3) to collapse and thus results in a pyramidal $S_{NP}(^1n\pi^*)$ minimum where the dihedral angle of C7−C6−O5−N3 is 133.8°. Meanwhile, the carbonyl group C6═O5 is significantly elongated from 1.23 Å in S_0 to 1.394 Å at the $S_{NP}(^1n\pi^*)$ minimum that leads to a diradical configuration. These structural changes in the evolution process are very similar to those in simple aliphatic and aromatic amides staring from the Franck−Condon region of an n→π* transition.[6,7]

The CASSCF/CASPT2/Amber calculations reveal that the 133.5 kcal/mol photon energy promotes the tetrapeptide to instantaneously populate the FC region of the $S_{NP}(^1n\pi^*)$ surface. This vertical excitation energy is similar to our previously calculated value (5.8 ev) at the CASSCF/MRSDCI level of theory for a simple aliphatic amide upon an n→π* transition in the gas phase.[6] These findings indicate that there is no significant blue-shift or red-shift for the n→π* transition of the amide unit in the solution matrix. Unlike a π→π* excitation, an accurate determination of the effect of the solvent on the n→π* transition of the amide unit is difficult.[47] The π→π* excitation of an amide unit has some charge transfer that has more favorable interaction with a polar solvent.[48,49] However, the n→π* transition of an amide unit ultimately leads to a diradical configuration,[6,7] which

is very insensitive to the polarity of solvents. By using some continuum solvent models, several groups[50−52] confirmed a red-shift phenomena for $\pi\rightarrow\pi^*$ transitions of amides, but no blue-shift was found for $n\rightarrow\pi^*$ transitions; these results are consistent with the results from the present calculations employing theoretical models of a solvent box. Obviously, the observed blue shift[53] of $n\rightarrow\pi^*$ transitions arises as a result of hydrogen bonding between the carbonyl group of an amide unit and the solvent. Further evidence comes from the fact that no blue shift is observed in non-hydrogen bonding solvents.[54] Both theoretical models employing a continuum or a solvent box can not fully account for the mutual interaction of the hydrogen bonding between an amide unit and the solvent. A theoretical model using a hydrogen bonding complex could better describe this mutual interaction. The solvent effect using the model of a solvent box is separately considered in this work, since the blue shift of the $n\rightarrow\pi^*$ transition of an amide unit does not lie at the heart of the photodegradation of peptides/proteins in solutions. The combined model using a hydrogen bonding complex and the solvent box will be chosen to explicitly describe this complicated mutual interaction in a subsequent project.

Compared with the simple aliphatic amides, the relaxation for the tetrapeptide on the $^1n\pi^*$ surface must overcome two barriers and use energy consumption for breaking hydrogen bonds between H1 and O2(TS_H) as well as N3−C6 (TS_{C-N}). As illustrated in Figure 1, TS_H and TS_{C-N} both lie in almost the same contour line with the 135.0 kcal/mol barrier with respect to the zero level of the ground state. It should be noted that, although TS_H is assigned to be the barrier for the collapse of a hydrogen bond, the energy consumption for increasing the distance of the C3−N6 bond from 1.42 ($S_{NP}(^1n\pi^*)$ minimum) to 1.70 Å (TS_H) also contributes to the local maximum of TS_H and vice versa for TSC-N. The energy consumption for breaking the H1···O2 hydrogen bond is determined to be approximately 11.0 kcal/mol by deduction of the components from the barrier for the C−N fission on the $S_{NP}(^1n\pi^*)$ surface (∼10.0 kcal/mol).[6,7] By using UV/IR double resonance spectroscopy, Mons and co-workers recently observed the stabilization energy for formation of a folded β-turn by linkage of the C═O···HN hydrogen bond to be 3400 cm^{-1} (9.7 kcal/mol) in a short peptide.[55] Our calculations provide a reasonable description for β-turn stabilization energy in small peptides as found in the experimental observations.

The two-dimensional model dominates the high energy excitation relaxation pathway. As shown in Figure 1, both the C7−C6−O5 angle and the C6−N3 distance are significantly increased along the decay pathway of the $n\rightarrow\pi^*$ transition for an amide chromophore. The C7−C6−O5 angle is significantly increased from 112.6° in the $S_{NP}(^1n\pi^*)$ minimum to 139.8° in the maximum of TS_{C-N} in concomitance with an elongation of the N3−C6 distance. Finally, this angle is enlarged to be 164.3°, where the distance of N3−C6 is 3.20 Å relaxing to the degenerate energy region of CI (S_{NP}/S_0), that is, 17.7 kcal/mol lower in energy than that of the FC point. The tetrapeptide is photoexcited to the Franck−Condon region of the $S_{NP}(^1n\pi^*)$ surface upon 193 nm UV light excitation and rapidly relaxes to the minimum of S_{NP} with a gradual increase in the carbonyl C═O bond length in the amide unit. The planar unit of the peptide is destroyed during this decay process, which causes a weakening of the α C−N bond due to lower $p-\pi$ conjugation. It is well accepted that the Norrish type I reaction (α bond fission) could take place with high efficiency once the carbonyl group is excited to the $^1n\pi^*$ energy surface. The energy consumption for the C−N fission for simple amides[6,7] and the tetrapeptide in this work is determined to be less than 10.0 kcal/mol in the $^1n\pi^*$ excited state by ab initio calculations at a high level of theory. The femtosecond photolysis of aqueous formamide conducted by Keiding[16] and his co-workers revealed that relaxation processes of simple amides in solution upon 193 nm UV light excitation are completed within a 10−20 ps time scale. In comparison with simple amides, the molecule of the tetrapeptide needs to consume more than ∼10.0 kcal/mol energy to overcome the interaction of the hydrogen bond between H1···O2. Fortunately, TS_H and TS_{C-N} do not lie in the same region of the reaction coordinate of the C−N distance (Figure 1), which avoids overlay between the two barriers and allows the relaxation to occur smoothly.

With an increasing C−N distance, the tetrapeptide evolves into the phase of the diradical character where two singly occupied electrons localize in the region of the C and N atoms, respectively. Since these two singly occupied electrons originate from the C−N σ bond fission, they inevitably distribute in the plane of the peptide unit from the viewpoint of the orientation in the early phase of the diradical formation. Qualitatively, the C−N fission in the $^1n\pi^*$ excited state ultimately leads to adiabatically diradical products in its excited state. Our previous calculations revealed that an RCO radical in the first excited electronic state adopts a linear R(C)−C−O arrangement (the angle is 180°) in simple amides, which is totally different from the geometric structure in the ground state (angle is ∼120°).[6,7] Actually, one singly occupied electron around the C atom changes its orientation from parallel ($\tilde{X}$, A′) to vertical ($\tilde{A}$, A″) corresponding to the plane of the peptide unit once the radical pair is promoted to the excited state. The changes of the orientation of the singly occupied electrons force the R(C)−C−O angle to gradually enlarge. When this angle is increased to be ∼180° (the linear arrangement), there is no remarkable difference in the orientation for the singly occupied electrons. These orientation changes finally lead the tetrapeptide to relax to the region of degenerate energy. The conical intersection of CI (S_{NP}/S_0) functions as an efficient nonadiabatic relay, leading the tetrapeptide to decay to the ground state. As discussed in our previous work,[6,7] there are two relaxation channels to account for the fate of the photodissociation of simple amides starting from the conical intersection between the $^1n\pi^*$ excited state and the ground state. Although relaxation to a hot molecule and a final product of the radical pair have almost the same probability from the viewpoint of theory, recent real time experimental results concluded that a smaller faction of the excited amides in solution dissociates to the RHO and NH_2 radical pairs, of which 50% escape recombination.[16] Considering that there is a strong hydrogen bond interaction between H1 and O2, a much lower yield of RHO and NHR is expected to be observed for a solvated tetrapeptide, and relaxation to a hot molecule could be the predominant decay channel upon high energy excitation that targets the −CO−NH− chromophore.

Time-Resolved Energy Transport Starting from the CI (S_{NP}/S_0). To provide insight into the decay processes that occur after reaching the CI (S_{NP}/S_0) point, we ran a 30 ps semiempirical QM/MM MD simulation (see Computational Details and Supporting Information for details). The recombination of the C3−N6 bond was achieved in a few femtoseconds, followed by relaxation to the hot ground state (S_0*) with more than 110.0 kcal/mol (energetic difference between FC point and CI (S_{NP}/S_0)) of excess heat. The energy transport along the peptide backbone was monitored by semiempirical QM/MM MD simulations, and this is illustrated in Figure 2. More than 110.0 kcal/mol of heat within 0.1 ps rapidly accumulates in the region

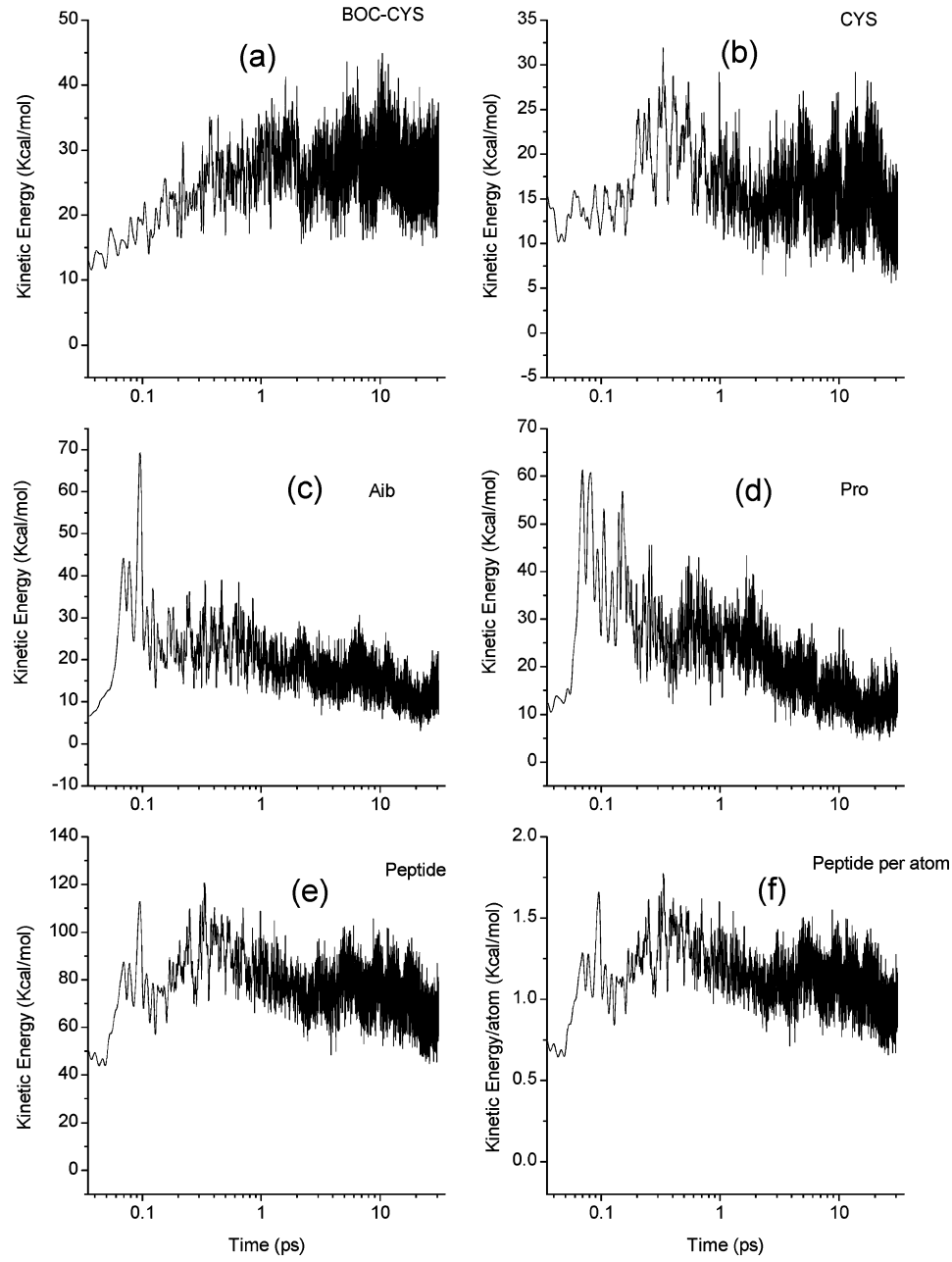

Figure 2. A simple schematic diagram depicting the time evolution of the kinetic energy of tetrapeptide starting from CI (S_{NP}/S_0) is shown. The upper two panels show the kinetic energy of the individual residues: (a) for Boc-Cysteine residue; (b) for Cysteine residue; (c) for α-aminoisobutyric (Aib) residue; (d) for Proline residue. The lowest panel presents the time evolution of the total kinetic energy (e) and kinetic energy per atom (f) along the peptide backbone.

of the dipeptides of Aib-Pro, which is the target of the photoexcitation. A high energy gradient drives the excess energy to be rapidly redistributed to the surrounding solvent molecules as well as to the vibrational modes of the peptide via intramolecular vibrational relaxation. The energy redistribution on the Boc-Cyc and Cyc-OMe residues evolves into a period of equilibration within 3.0 ps inconcomitance with a substantial decrease in the energy distribution in the region of the dipeptides of Aib-Pro (see the upper panel in Figure 2). Finally, 27.2 and 15.4 kcal/mol excess energy (mean kinetic energy in the time span from 3 to 30 ps) distributes the Boc-Cyc and Cyc-OMe residues (disulfide bond region), respectively. Figure 2f shows the time evolution of kinetic energy per atom. The excess energy is ranged by 1.0−2.0 kcal/mol along per atom. This means that the less than 4.0 kcal/mol vibrational energy relaxes in the S−S bond during the thermalization process, and the transient temperature is only slightly above the solvent temperature. Therefore, the process of thermalization after high-energy excitation of the amide chromophore can not significantly cause the S−S bond to weaken. It can be clearly seen from the lowest panel in Figure 2 that the most drastic dissipation into the solvent takes place in a narrow time window after 0.1 ps. The high efficiency of this process is vital for biomolecules to avoid an overheated environment.[56] Compared with the fast energetic dissipation into the solvent, the propagation of the heat along the peptide backbone takes place on a relatively longer time scale (∼3 ps). The amount of the dissipation energy into the solvent is roughly represented by the energetic discrepancy between the total excess heat in the hot ground state molecule (∼110.0 kcal/mol) and the total kinetic energy along the peptide backbone.

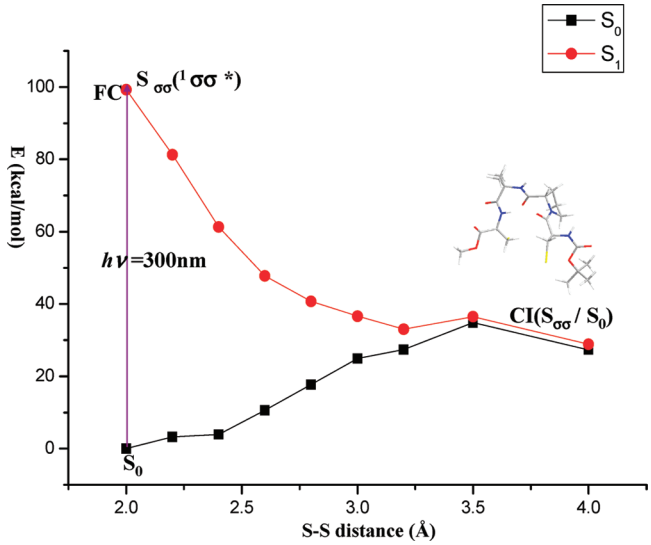

Figure 3. Schematic diagram of the energy profiles along the relaxation pathways for low energy excitation (300 nm) along the repulsive $S_{\sigma\sigma}(^1\sigma\sigma^*)$ surface.

Up to 3 ps, approximately 60% of the excess energy is dissipated into the solvent. On the longer time scale, more energy will dissipate into the solvent so that the dissipation rate may reach Hamm and co-workers' estimation (~70%).[56] The processes of energy transport (vibrationally excitation) and fast dissipation to solvent for formamide were also well monitored by time-resolved absorption spectroscopy.[16] It was found that the majority of the excited formamide molecules decayed to the ground state within 1 psm and subsequent energy transport (vibrationally excitation) was confirmed by a strong red shift of the ground state absorption signals.[16] The dissipation to the solvent is complete within 10 ps, which is determined by the observed blue shifts toward the ground state absorption spectrum.[16]

Low-Energy Excitation (300 nm) Relaxation Pathway along S−S Bond Fission. As shown in Figure 3, the photoexcitation of the tetrapeptide by 300 nm UV light initiates the relaxation along the repulsive $S_{\sigma\sigma}(^1\sigma\sigma^*)$ state starting from the Franck−Condon region. The intrinsic force of the repulsive state drives S−S to separate along a steep downward pathway that ultimately leads to a CI ($S_{\sigma\sigma}/S_0$). The amount of energy is decreased significantly (by more than 60.0 kcal/mol) upon going from the FC to the CI ($S_{\sigma\sigma}/S_0$) while the S−S bond distance is increased from 2.0 to 3.5 Å. However, the energy level is remarkably increased while the S−S distance is elongated on the ground state potential surface. Finally, the energetic level reaches maximum of ground state and intersects with the $S_{\sigma\sigma}(^1\sigma\sigma^*)$ surface (CI ($S_{\sigma\sigma}/S_0$)), which has a diradical configuration and two singly occupied electrons localizes in the region of the two sulfur atoms of the cysteine residue, respectively.

Fast Unfolding−Refolding Events Powered by the Driving Force of the Solvent Starting from CI ($S_{\sigma\sigma}/S_0$). The conformational change that takes place starting from ($S_{\sigma\sigma}/S_0$) was characterized by semiempirical QM/MM MD simulations. Although the H1−O2 hydrogen bond is partially weakened in the photochemical step, the tetrapeptide still exhibits β-turn architecture at the beginning of the MD simulations. Three typical conformational changes are observed: (a) the recombination of the S−S bond leads to the original architecture of β-turn; (b) iteration of unfolding and refolding of the β-turn architecture; (c) unfolding of the β-turn architecture followed by folding of the 3_{10}-helix structure. Figure 4 gives the time evolution of the

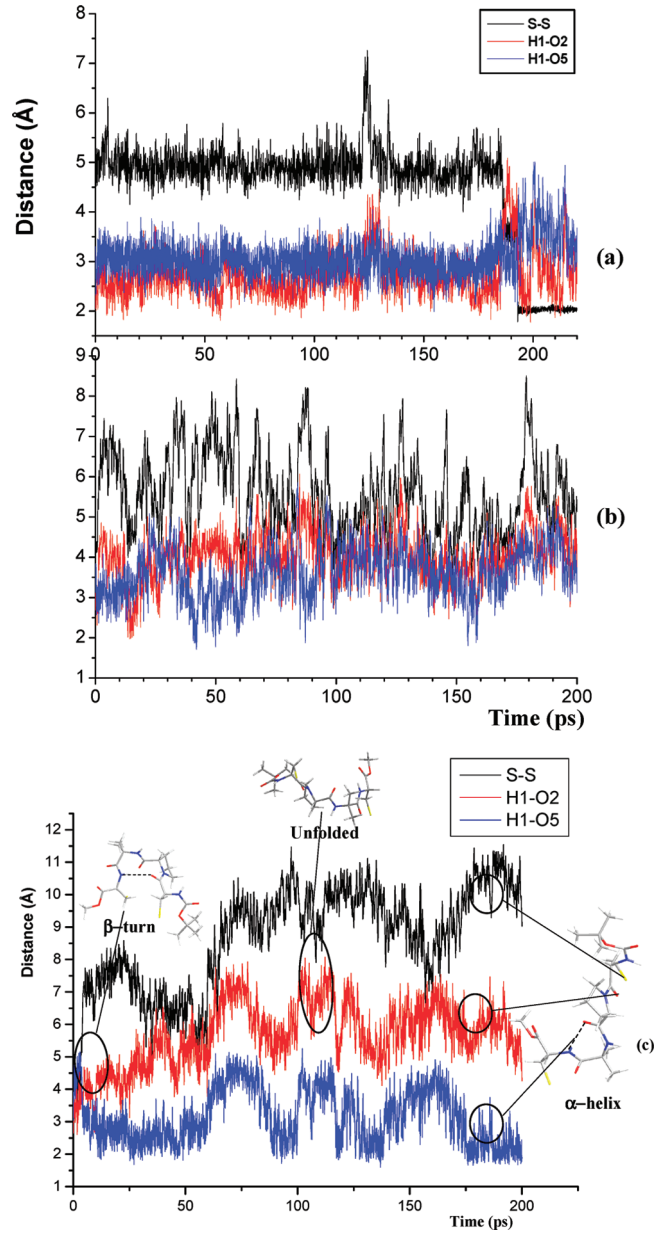

Figure 4. A schematic diagram of the time evolution of the conformational changes for the tetrapeptide starting from CI ($S_{\sigma\sigma}/S_0$) is shown: (a) the recombination of the S−S bond that leads to the original architecture of the β-turn; (b) iteration of unfolding and refolding of the β-turn architecture; (c) unfolding of the β-turn architecture followed by folding of the 3_{10}-helix structure.

S−S, H1−O2, and O1−O5 distances. The case of iteration of the unfolding and refolding of the β-turn (b) is the most common event in present MD simulations. In conformation change (a), the distances of bonds S−S, H1−O2, and O1−O5 just fluctuate around their initial values in the time span from 0−200 ps. The S−S distance gradually decreases after 200 ps and relaxes to its original value around 2.0 Å in the final phase of the MD simulations. Meanwhile, hydrogen bond H1−O2 goes back to its original intensity, which defines well the rigid β-turn architecture. In this case, the exchanged energy from solvent powers the thermal motion of the peptide and continues to propel the peptide to adopt a diradical structure in the early phase of the MD simulations. Since the peptide ends of the cysteinyl diradical could not get enough energy to power unfolding, the S−S bond undergoes a recombination relaxing to its original architecture in concomitance with the decayed amount of

exchanged energy from the solvent. This kind of radical recombination is not an uncommon phenomenon in peptide dynamics.[22] In conformation change (b), the S−S and H1−O2 bonds both repeat elongation and reduction, i.e., the β-turn architecture unfolds and refolds. In this case, the peptide must exchange energy with the solvent iteratively so as to provide a driving force for the unfold−refold transition. The most interesting conformation change is the case of (c). We found that the S−S distance increases and approaches a maximum equilibrium (9−10 Å) value within about 100 ps. The increased S−S distance results in a weakened H1−O2 hydrogen bond when the time evolution reaches 120 ps. The long distance of H1−O2 (e.g., 6−7 Å) indicates that the β-turn is completely opened within 120 ps. This time scale does not include the time of the photochemical step, so our theoretical value appears likely to be comparable to that of Hamm and co-workers' experimental observations (160 ps) but is shorter than that of the nonequilibrium MD simulations (240 ps).[24] Obviously, the unfolded tetrapeptide is not in its stabilized state, and it inevitably relaxes to another more stable isomer on a longer time scale. The conformational changes are mainly associated with decreasing the H1−O5 bond length in the time evolution spanning from 120 to 200 ps. Up to 200 ps, the distance of the H1−O5 bond length is significantly decreased to be around 1.8 Å in concomitance with a slight shortening of the H1−O2 distance (∼4.5 Å). The strong hydrogen bond between the i and i+2 residues (H1−O5) defines a 3_{10}-helix structural architecture fairly well in the final phase of the MD simulations. To complete such a conformational change, the peptide must gain more energy from the solvent than those in cases (a) and (b).

Hochstrasser and his co-workers observed that the S−S bond was broken in <200 fs, and the approximately 70−80% of liberated thiyl radicals underwent geminate recombination.[21,23] Nevertheless, the relatively higher yield of β-turn opening was observed by Hamm within a similar time scale (∼160 ps).[24,25] The conformational change of case (a) conducted by semiempirical QM/MM MD simulation presents a dynamic process of recombination of thiyl radicals. Case (c) reproduced the β-turn opening within the experimentally observed time scale, whereas case (b) provides the dynamic process of the "transition state" between cases (a) and (c), in which the iteration of the unfolding and refolding of β-turn occurs. Since atomic velocities were randomly initialized with Maxwell distribution at a given temperature, the different initial velocities simulate the various amounts of energy exchange between solvent and peptide. The amount of vibrational energy from the solvent is successively increased from case (a) to case (c), which drives the different cases of conformal changes from (a) recombination of thiyl radicals via the "transition state" of (b) iteration of unfolding and refolding of β-turn to (c) β-turn opening. The discrepancy of efficiency of energy exchange between peptide and solvent significantly influences the yield of β-turn opening as shown by the different experimental observations between Hochstrasser and Hamm. Therefore, the efficiency of energy exchange between peptide and solvent is the dominant factor of yield of the β-turn opening of a peptide after the photochemical step.

Experimentally, the disulfide bond as an ideal optical trigger unit has been incorporated into a short peptide to better understand the principle mechanisms behind fast peptide/protein folding/unfolding.[21−23] The disulfide bond in these peptides is known to be broken in less than 100 ps after excitation by an ultrashort UV laser pulse, which provides a fast trigger for protein folding or unfolding.[57−60] Photocleavage of a disulfide bond on the picosecond time scale could remove the constraint of the linkage of peptide ends by an aryl disulfide cross-linking-group, which allows the earliest events of helix formation in a short peptides to be observed.[61] As another example of the fast initiation of peptide unfolding/refolding processes triggered by the photocleavage of a disulfide bond, the detailed dynamical information of the unfolding−refolding events for cyclo(Boc-Cys-Pro-Aib-Cys-OMe) have been characterized by our present semiempirical QM/MM MD simulations. The time scale of the MD simulation for the unfolding processes (e.g., the β-turn opening) is in good agreement with experimental observations.

Unlike free radicals, thiyl radicals in peptide ends are tethered together and can not escape from each other. The recombination of the thiyl radical in peptide ends is controlled by the motion of the peptide backbone.[59] On the other hand, the solvent cage around the cysteinyl radicals also play an important role in the processes associated with the combination of cysteinyl radicals. We also attempted to perform MD simulations in the gas phase (with no solvent involved), and the cysteinyl radicals were observed to recombine on the sub-100 fs time scale. This indicates that there is no way for the β-turn to open without solvent participation. Once cysteinyl radicals are generated, the polar solvent of methanol molecules rapidly diffuses around the radicals forming a solvent cage. The strong electrostatic interactions keep the thiyl radicals together and weaken and reduce the possibility of close contact in a physical sense. This is why the recombination of the thiyl radical of a peptide in a solvent takes place on a longer time scale, while it happens on the sub-100 fs time scale when there is no solvent participation (as in the gas phase). Moreover, the motion and reorientation of the solvent molecules dominates the processes associated with the unfolding−refolding.[62] Frauenfelder and co-workers called this dominant factor slaving, which is a descriptor for large scale protein motions followed by solvent fluctuations with a slower rate coefficient.[62] Photoexcitation initiates the motion of the tetrapeptide (structural changes), which further induces the fluctuation of solvent. The rebirth of a new hydrogen bonding pattern stabilizes the unfolded−refolded tetrapeptide. The mutual interaction between the peptide and the solvent molecules powers the unfolding−refolding to occur step by step. As mentioned above, more than 60% of the energy is dissipated into the solvent in the process of energy transport, and this is enough to trigger conformational changes after the photochemical steps. The solvent functions as an energy reservoir to power the transition from the β-turn to the 3_{10}-helix structure. However, what controls the folding rate is hotly debated. This is a very complicated issue. Herein, we only present semiempirical QM/MM MD simulations of the unfolding−refolding after the photochemical steps to understand the final fate of excited energy. More experiments and theoretical calculations are needed to explore the role of the solvent in the peptide/proteins folding and unfolding processes.

Conclusions

The present case study describes the mechanisms of the photoinduced C−N of the amide unit and S−S bond fission of the cyclic tetrapeptide in a methanol solvent. In the case of high-energy excitation (<193 nm), the carbonyl group of the peptide unit is excited, and this promotes the tetrapeptide to instantaneously populate the $^1n\pi^*$ surface. A two-dimensional model of the reaction coordinates (C−N distance and C−C−O angle in peptide unit) controls the relaxation from the FC of the $n\rightarrow\pi^*$ transition. The tetrapeptide molecule upon high energy excitation overcomes two barriers with ∼10.0 kcal/mol, respectively, and uses energy consumption for breaking hydrogen bonds between

H1 and O2(TS_H) as well as N3−C6 (TS_{C-N}), ultimately leading to the ground state via the conical intersection of CI (S_{NP}/S_0). Following this point, the relaxation to a hot molecule with the original structure in the ground state is the predominant decay channel. The hot molecule (S_0*) has ∼110.0 kcal/mol excess energy, which is rapidly redistributed to the surrounding solvent molecules as well as to the vibrational modes of the peptide via intramolecular vibrational relaxation. The energy transport is characterized by the present semiempirical QM/MM/MD simulations. A large amount of heat (∼110.0 kcal/mol) is initially accumulated in the region of the targeted point of the photoexcitation, and more than 60% of the heat is rapidly dissipated into the solvent on the femtosecond time scale. The relatively slower propagation of heat along the peptide backbone reaches a phase of equilibration within 3 ps.

Excitation with 300 nm UV light initiates the relaxation along the repulsive $S_{\sigma\sigma}$ ($^1\sigma\sigma$*) state and directly decays to the CI ($S_{\sigma\sigma}/S_0$) in concomitance with a separation of the disulfide bond. The unfolding-refolding events are powered by the driving force of the solvent following the photochemical steps. Once cysteinyl radicals are generated, the polar solvent of methanol molecules rapidly diffuses around the radicals forming a solvent cage and reducing the possibility of close contact in a physical sense. The fast unfolding−refolding event is triggered by S−S bond fission and powered by the dramatically thermal motion of solvent that benefits from heat dissipation. The secondary structural changes of the tetrapeptide can be understood in terms of the evolution of the hydrogen bonds H1−O2 and H1−O5 (associated with the first structure). Our MD simulations conclude that the β-turn opening can be achieved in 120 ps (vs experimental observations with a total time scale of 160 ps) without the inclusion of the time associated with the photochemical steps, and eventually relaxes to a 3_{10}-helix structural architecture within 200 ps. The present work provides an overview of the hydrogen bond dynamics triggered by the photoinduced fission of disulfide bonds so as to better understand the associated unfolding−refolding events in peptides/proteins.

Acknowledgment. We thank Prof. Massimo Olivucci (X.C.'s postdoctoral supervisor) for instructive discussions on the topic of photodegradation of peptides that is involved in this paper. This work was financially supported by the following grants: FANEDD200932 and NSFC20973025 (to X.C.), NSFC20873007 (to L.G.), NSFC 20720102038 and Major State Basic Research Development Programs 2004CB719903 (to W.F.) and Hong Kong Research Grants Council (HKU/7039/07P) (to D.L.P.).

Supporting Information Available: Section 1: Computational details; Table S2: The Energy Differences in kcal/mol and the Absolute Energy in Hartees for the Optimized Structures; Section 2: Cartesian Coordinates for the Optimized Structures for the Tetrapeptide in the Methanol Box. This material is available free of charge via the Internet at http://pubs.acs.org.

References and Notes

(1) Hershko, A.; Ciechanover, A.; Rose, I. A. *Proc. Natl. Acad. Sci. U.S.A.* **1979**, *76*, 3107–3110.
(2) Ciechanover, A.; Heller, H.; Elias, S.; Haas, A. L.; Hershko, A. *Proc. Natl. Acad. Sci. U.S.A.* **1980**, *77*, 1365–1368.
(3) Hershko, A.; Ciechanover, A.; Heller, H.; Haas, A. L.; Rose, I. A. *Proc. Natl. Acad. Sci. U.S.A.* **1980**, *77*, 1783–1786.
(4) Hershko, A.; Ciechanover, A. *Annu. Rev. Biochem.* **1982**, *51*, 335–364.
(5) Sionkowska, A. *J. Photochem. Photobiol., A* **2006**, *117*, 61–67, and references cited therein.
(6) Chen, X. B.; Fang, W. H.; Fang, D. C. *J. Am. Chem. Soc.* **2003**, *125*, 9689–9698.
(7) Chen, X. B.; Fang, W. H. *J. Am. Chem. Soc.* **2004**, *126*, 8976–8980.
(8) Volman, D. H. *J. Am. Chem. Soc.* **1941**, *63*, 2000–2002.
(9) Hayon, E.; Nakashima, M. *J. Phys. Chem.* **1971**, *75*, 1910–1914.
(10) Liu, D.; Fang, W. H.; Fu, X. Y. *Chem. Phys. Lett.* **2000**, *318*, 291–297.
(11) Park, J.; Ha, J. H.; Hochstrasser, R. M. *J. Chem. Phys.* **2004**, *121*, 7281–7292.
(12) Lundell, J.; Krajewska, M.; Rasanen, M. *J. Phys. Chem. A* **1998**, *102*, 6643–6650.
(13) Back, R. A.; Boden, J. C. *Trans. Faraday Soc.* **1971**, *69*, 88.
(14) Kakumoto, T.; Saito, K.; Imamura, A. *J. Phys. Chem.* **1985**, *89*, 2286–2291.
(15) Forde, N. R.; Butler, L. J.; Abrash, S. A. *J. Chem. Phys.* **1999**, *110*, 8954–8968.
(16) Petersen, C.; Dahl, N. H.; Jensen, S. K.; Thgersen, J.; Keiding, S. R. *J. Phys. Chem. A* **2008**, *112*, 3339–3344.
(17) Schmidt, B.; Hogg, P. J. *BMC Struct. Biol.* **2007**, *7*, 49–61.
(18) Jakob, U.; Muse, W.; Eser, Bardwell, J. C. *Cell* **1999**, *96*, 341–352.
(19) Lee, C.; Lee, S. M.; Mukhopadhyay, P.; Kim, S. J.; Lee, S. C.; Ahn, W. S.; Yu, M. H.; Storz, G.; Ryu, S. E. *Nat. Struct Mol. Biol.* **2004**, *11*, 1179–1185.
(20) Yang, Y.; Song, Y. L.; Loscalzo, J. *Proc. Natl. Acad. Sci. U.S.A.* **2007**, *104*, 10813–10817.
(21) Lu, H. S. M.; Volk, M.; Kholodenko, Y.; Gooding, E.; Hochstrasser, R. M.; DeGrado, W. F. *J. Am. Chem. Soc.* **1997**, *119*, 7173–7180.
(22) Volk, M. *Eur. J. Org Chem.* **2001**, 2606–2621, and references cited therein.
(23) Volk, M.; Kholodenko, Y.; Lu, H. S. M.; Gooding, E. A.; DeGrado, W. F.; Hochstrasser, R. M. *J. Phys. Chem. B* **1997**, *101*, 8607–8616.
(24) Kolano, C.; Helbing, J.; Kozinski, M.; Sander, W.; Hamm, P. *Nature* **2006**, *444*, 469–472.
(25) Kolano, C.; Helbing, J.; Bucher, G.; Sander, W.; Hamm, P. *J. Phys. Chem. B* **2007**, *111*, 11297–11302.
(26) Nöting, B.; Golbik, R.; Fersht, A. R. *Proc. Natl. Acad. Sci. U.S.A.* **1995**, *92*, 10668–10672.
(27) Phillips, C. M.; Mizutani, Y.; Hochstrasser, R. M. *Proc. Natl. Acad. Sci. U.S.A.* **1995**, *92*, 7292–7296.
(28) Ballew, R. M.; Sabelko, J.; Gruebele, M. *Proc. Natl. Acad. Sci. U.S.A.* **1996**, *93*, 5759–5764.
(29) Balakrishnan, G.; Hu, Y.; Case, M. A.; Spiro, T. G. *J. Phys. Chem. B* **2006**, *110*, 19877–19883.
(30) Mikhonin, A. V.; Asher, S. A. *J. Am. Chem. Soc.* **2006**, *128*, 13789–13795.
(31) Jas, G. S.; Eaton, W. A.; Hofrichter, J. *J. Phys. Chem. B* **2001**, *105*, 261–272.
(32) Ervin, J.; Sabelko, J.; Gruebele, M. *J. Photochem. Photobiol. B* **2000**, *54*, 1–15.
(33) Bredenbeck, J.; Helbing, J.; Sieg, A.; Schrader, T.; Zinth, W.; Renner, C.; Behrendt, R.; Moroder, L.; Wachtveitl, J.; Hamm, P. *Proc. Natl. Acad. Sci. U.S.A.* **2003**, *100*, 6452–6457.
(34) Bredenbeck, J.; Helbing, J.; Behrendt, R.; Renner, C.; Moroder, L.; Wachtveitl, J.; Hamm, P. *J. Phys. Chem. B* **2003**, *107*, 8654–8660.
(35) Helbing, J.; Bregy, K.; Bredenbeck, J.; Pfister, R.; Hamm, P.; Huber, R.; Wachtveitl, J.; De Vico, L.; Olivucci, M. *J. Am. Chem. Soc.* **2004**, *126*, 8823–8834.
(36) Andruniow, T.; Fantacci, S.; Angelis, F. D.; Ferre, N.; Olivucci, M. *Angew. Chem., Int. Ed.* **2005**, *44*, 6077–6081.
(37) Case, D. A.; Pearlman, D. A.; Caldwell, J. W.; Cheatham, T. E., III.; Ross, W. S.; Simmerling, C. L.; Darden, T. A.; Merz, K. J.; Stanton, R. V.; Cheng, A. L.; Vincent, J. J.; Crowley, M.; Tsui, V.; Radmer, R. J.; Duan, Y.; Pitera, J.; Massova, I.; Seibel, G. L.; Singh, U. C.; Weiner, P. K.; Kollman, P. A. *AMBER 6*; University of California: San Francisco, 1999.
(38) Feller, S. E.; Zhang, Y. H.; Pastor, R. W.; Brooks, B. R. *J. Chem. Phys.* **1995**, *103*, 4613–4621.
(39) Phillips, J. C.; Braun, R.; Wang, W.; Gumbart, J.; Tajkhorshid, E.; Villa, E.; Chipot, C.; Skeel, R. D.; Kale, L.; Schulten, K. *J. Comput. Chem.* **2005**, *26*, 1781–1802.
(40) Humphrey, W.; Dalke, A.; Schulten, K. *J. Mol. Graphics* **1996**, *14*, 33–38.
(41) Frisch, M. J.; Trucks, G. W.; Schlegel, H. B.; Scuseria, G. E.; Robb, M. A.; Cheeseman, J. R.; Montgomery, J. A., Jr.; Vreven, T.; Kudin, K. N.; Burant, J. C.; Millam, J. M.; Iyengar, S. S.; Tomasi, J.; Barone, V.; Mennucci, B.; Cossi, M.; Scalmani, G.; Rega, N.; Petersson, G. A.; Nakatsuji, H.; Hada, M.; Ehara, M.; Toyota, K.; Fukuda, R.; Hasegawa, J.; Ishida, M.; Nakajima, T.; Honda, Y.; Kitao, O.; Nakai, H.; Klene, M.; Li, X.; Knox, J. E.; Hratchian, H. P.; Cross, J. B.; Adamo, C.; Jaramillo, J.; Gomperts, R.; Stratmann, R. E.; Yazyev, O.; Austin, A. J.; Cammi, R.; Pomelli, C.; Ochterski, J. W.; Ayala, P. Y.; Morokuma, K.; Voth, G. A.; Salvador, P.; Dannenberg, J. J.; Zakrzewski, V. G.;

Dapprich, S.; Daniels, A. D.; Strain, M. C.; Farkas, O.; Malick, D. K.; Rabuck, A. D.; Raghavachari, K.; Foresman, J. B.; Ortiz, J. V.; Cui, Q.; Baboul, A. G.; Clifford, S.; Cioslowski, J.; Stefanov, B. B.; Liu, G.; Liashenko, A.; Piskorz, P.; Komaromi, I.; Martin, R. L.; Fox, D. J.; Keith, T.; Al-Laham, M. A.; Peng, C. Y.; Nanayakkara, A.; Challacombe, M.; Gill, P. M. W.; Johnson, B.; Chen, W.; Wong, M. W.; González, C.; Pople, J. A. *Gaussian03*, revision D.02; Gaussian, Inc.: Pittsburgh, PA, 2004.

(42) Andersson, K.; Barysz, M.; Bernhardsson, A.; Blomberg, M. R. A.; Carissan, Y.; Cooper, D. L.; Cossi, M.; Fleig, T.; Fülscher, M. P.; Gagliardi, L.; de Graaf, C.; Hess, B. A.; Karlström, G.; Lindh, R.; Malmqvist, P.-Å.; Neogrády, P.; Olsen, J.; Roos, B. O.; Schimmelpfennig, B.; Schütz, M.; Seijo, L.; Serrano-Andrés, L.; Siegbahn, P. E. M.; Stålring, J.; Thorsteinsson, T.; Veryazov, V.; Wierzbowska, M.; Widmark, P. O. *MOLCAS*version 7.1; University of Lund: Sweden, 2008.

(43) Ponder, J.; Richards, W. F. M. *J. Comput. Chem.* **1987**, *8*, 1016–1024.

(44) Ferré, N.; Cembran, A.; Garavelli, M.; Olivucci, M. *Theor. Chem. Acc.* **2004**, *112*, 335–341.

(45) (a) Stewart, J. J. P. *J. Mol. Model.* **2007**, *13*, 1173–1213. (b) MOPAC (Molecular Orbital PACkage), http://openmopac.net/ (Accessed March 2010).

(46) (a) Kretsinger, R. H. *Nat. Struct. Biol.* **1997**, *4*, 514–516. (b) Borics, A.; Murphy, R. F.; Lovas, S. *Biopolymers* **2006**, *85*, 1–10.

(47) Besley, N. A.; Oakley, M. T.; Cowan, A. J.; Hirst, J. D. *J. Am. Chem. Soc.* **2004**, *126*, 13502–13511.

(48) Nielsen, E. B.; Schellman, J. A. *J. Phys. Chem.* **1967**, *71*, 2297–2304.

(49) Besley, N. A.; Hirst, J. D. *J. Phys. Chem. A* **1998**, *102*, 10791–10797.

(50) DelBene, J. E. *J. Chem. Phys.* **1975**, *62*, 1961–1970.

(51) Sobolewski, A. L. *Photochem. Photobiol.* **1995**, *89*, 89–97.

(52) Kauss, M.; Webb, S. P. *J. Chem. Phys.* **1997**, *107*, 5771–5775.

(53) Rocha, W. R.; Martins, V. M.; Coutinho, K.; Canuto, S. *Theor. Chem. Acc.* **2002**, *108*, 31–37.

(54) Bash, H.; Robin, M. B.; Kuebler, N. A. *J. Chem. Phys.* **1968**, *49*, 5007–5018.

(55) Brenner, V.; Piuzzi, F.; Dimicoli, I.; Tardivel, B.; Mos, M. *Angew. Chem., Int. Ed.* **2007**, *46*, 2463–2466.

(56) Botan, V.; Backus, E. H. G.; Pfister, R.; Moretto, A.; Crisma, M.; Toniolo, C.; Nguyen, P. H.; Stock, G.; Hamm, P. *Proc. Natl. Acad. Sci. U.S.A.* **2007**, *104*, 12749–12754.

(57) Scott, T. W.; Liu, S. N. *J. Phys. Chem.* **1989**, *93*, 13932–1396.

(58) Ernsting, N. P. *Chem. Phys. Lett.* **1990**, *166*, 221–226.

(59) Borisevich, N. A.; Lysak, N. A.; Melnichuk, S. V.; Tikhomirov, S. A.; Tolstorozhev, G. B. In *Ultrafast Phenomena in Spectroscopy*; Klose, E., Wilhelmi, B. , Eds.; Springer-Verlag: Berlin/ Heidelberg, 1990; Vol. 49, pp 276−281.

(60) Hirata, Y.; Niga, Y.; Okada, T. *Chem. Phys. Lett.* **1994**, *221*, 283–288.

(61) Marqusee, S.; Robbins, V. H.; Baldwin, R. L. *Proc. Natl. Acad. Sci. U.S.A.* **1989**, *86*, 5286–5290.

(62) Frauenfelder, H.; Fenimore, P. W.; Chen, G.; Mcmahon, B. H. *Proc. Natl. Acad. Sci. U.S.A.* **2006**, *103*, 15469–14472.

JP1003616